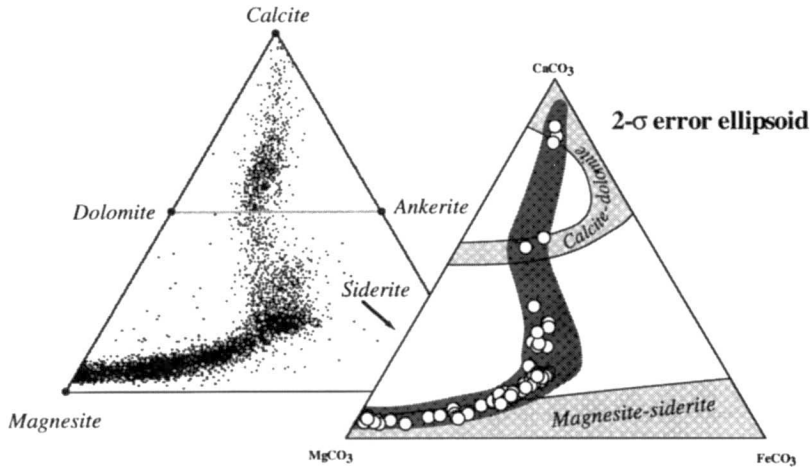

FIG. 3 Carbonate compositions in ALH84001. Left, 6,736 semi-quantitative analyses form two individual carbonate regions in ALH84001. Note that pixel size and carbonate grain size are nearly identical, so that many individual analyses represent compositions on the border of two grains. Right, 700 °C ternary phase diagram[11]. Quantitative analyses are shown as white circles, dark-shaded area shows compositions seen on the left.

hydrous phases, suggest that impact-driven metasomatism may be an important source of carbonate mineral production on Mars. Martian carbonates, rather than being deposited by an actively circulating, long-lived water-rich system, may instead have been produced during isolated, short-term cycling of CO_2 within the ancient, impact-fractured crust. Over time this process may have globally redistributed carbonates throughout the shallow crust of Mars, possibly disguising carbonate deposits produced during collapse of an early CO_2-rich atmosphere. □

Received 5 October 1995; accepted 9 May 1996.

1. McSween, H. Y. Jr *Meteoritics* **29,** 757–779 (1994).
2. Score, R. & Lindstrom, M. *Ant. Meteorite Newsl.* **18(2),** 20 (1995).
3. Mittlefehldt, D. W. *Meteoritics* **29,** 214–221 (1994).
4. Harvey, R. P. & McSween, H. Y. Jr *Meteoritics* **29,** 472 (1994).
5. Treiman, A. H. *Meteoritics* **30,** 294–302 (1995).
6. Romanek, C. S. *et al. Nature* **372,** 655–657 (1994).
7. Romanek, C. S., Thomas, K. L., Gibson, E. K. Jr, McKay, D. S. & Socki, R. A. *Meteoritics* **30,** 567–568 (1995).
8. Jull, A., Eastoe, C. J., Xue, S. & Herzog, G. F. *Meteoritics* **30,** 311–318 (1995).
9. Wentworth, S. J. & Gooding, J. L. *Proc. lunar planet. Sci. Conf.* **XXVI,** 1489–1490 (1995).
10. Anovitz, L. M. & Essene, E. J. *J. Petrol.* **28,** 389–414 (1987).
11. Woods, T. L. & Garrels, R. M. *Geochim. cosmochim. Acta* **56,** 3031–3043 (1992).
12. Trommsdorff, V. & Connolly, J. A. D. *Contr. Miner. Petrol.* **104,** 1–7 (1990).
13. Johannes, W. *Am. J. Sci.* **267,** 1083–1104 (1969).
14. Schreyer, W., Ohnmacht, W. & Mannchen, T. *Lithos* **5,** 345–364 (1972).
15. Cribb, S. J. *Norsk Geol. Tidsskrift* **62,** 161–168 (1982).
16. Ohnmacht, W. *J. Petrol.* **15,** 303–323 (1974).
17. James, P. B., Kieffer, H. H. & Paige, D. A. in *Mars* (eds Kieffer, H. H., Jakosky, B. M., Snyder, C. W. & Matthews, M. S.) 934–968 (Univ. Arizona Press, Tucson, 1992).
18. Martinez, I., Agrinier, P., Schärer, U. & Javoy, M. *Earth planet. Sci. Lett.* **121,** 559–574 (1994).
19. Ash, R. A., Knott, S. F. & Turner, G. *Meteoritics* **30,** 485 (1995).
20. Baker, V. R., Carr, M. H., Gulick, V. C., Williams, C. R. & Marley, M. S. in *Mars* (eds Kieffer, H. H., Jakosky, B. M., Snyder, C. W. & Matthews, M. S.) 493–522 (Univ. Arizona Press, Tucson, 1992).
21. Ridley, W. I., Plumlee, G. S., DeBraal, J. D. & Reed, M. H. *Meteoritics* **30,** 565 (1995).
22. Griffith, L. L. & Shock, E. L. *Nature* **377,** 406–403 (1995).

ACKNOWLEDGEMENTS. We thank L. Anovitz for helpful discussions, and A. Treiman, W. M. Murphy and O. Vidal for reviews. This work was supported by NASA (H.Y.M.) and NSF (R.P.H.).

CORRESPONDENCE should be addressed to R.P.H. (e-mail rph@po.cwru.edu).

Spectroscopic evidence for a pseudogap in the normal state of underdoped high-T_c superconductors

H. Ding*†, T. Yokoya‡, J. C. Campuzano*†, T. Takahashi‡, M. Randeria§, M. R. Norman†, T. Mochiku‖¶, K. Kadowaki‖¶ & J. Giapintzakis#

* Department of Physics, University of Illinois at Chicago, Chicago, Illinois 60607, USA
† Materials Science Division, Argonne National Laboratory, Argonne, Illinois 60439, USA
‡ Department of Physics, Tohoku University, Sendai 980, Japan
§ Tata Institute of Fundamental Research, Bombay 400005, India
‖ Institute of Materials Science, University of Tsukuba, Tsukuba, Ibaraki 305, Japan
¶ National Research Institute for Metals, Tsukuba, Ibaraki 305, Japan
# Department of Physics, University of Illinois at Urbana-Champaign, Urbana, Illinois 61801, USA

It is well known that BCS mean-field theory is remarkably successful in describing conventional superconductors. A central concept of BCS theory is the energy gap in the electronic excitation spectrum below the superconducting transition temperature, T_c. The gap also serves as the order parameter: quite generally, long-range phase coherence and a non-zero gap go hand-in-hand[1]. But in underdoped high-T_c superconductors there is considerable evidence that a pseudogap (a suppression of spectral weight) is already formed in the normal state above T_c—first, from studies of the spin excitation spectrum[2–5,24], which measure a 'spin gap', and later from a variety of other probes[6–10]. Here we present a study of underdoped $Bi_2Sr_2CaCu_2O_{8+\delta}$ (Bi2212) using angle-resolved photoemission spectroscopy (ARPES), which directly measures the momentum-resolved electron excitation spectrum of the CuO_2 planes. We find that a pseudogap with *d*-wave symmetry opens up in the normal state below a temperature $T^* > T_c$, and develops into the *d*-wave superconducting gap once phase coherence is established below T_c.

In ARPES, photons incident upon a sample cause electrons to be ejected, whose energies and momenta are measured. From this one obtains the electronic excitation spectrum of the sample. Our experiments were carried out at the Synchrotron Radiation Center, Wisconsin, following procedures described previously[11], with 19- or 22-eV photons at an energy resolution of 22–27 meV (full-width at half-maximum, FWHM) and an angular window of ±1°. Sample underdoping was achieved by adjusting the oxygen partial pressure during annealing of the float-zone grown crystals. These crystals have sharp X-ray diffraction rocking curves with structural coherence lengths of 1,250 Å, similar to the near optimally doped samples studied earlier. This high degree of order apparently also helps in maintaining the structural stability of the sample in an ultra-high vacuum of $< 4 \times 10^{-11}$ torr under constant-temperature cycling, even up to 300 K, without measurable sample degradation. All samples show a very flat surface after cleaving, which is essential for determining the intrinsic momentum (**k**) dependence of the gap.

We have studied several samples ranging from overdoped to underdoped, where optimal doping corresponds to a T_c of 92 K. In this Letter we will focus on a moderately underdoped sample with a T_c of 83 K (transition width 2 K), and a heavily underdoped sample with a T_c of 10 K (width >5 K), and contrast these results with a near-optimal (slightly overdoped) 87 K sample (width 1 K). We will simply label the samples by their onset T_cs.

It is important to separate the effects of changes in carrier concentration from those due to disorder. Because the superconducting gap for near-optimal Bi2212 is consistent with a *d*-wave order parameter[12–14], for which disorder leads to T_c reduction, we must ensure that the samples we call underdoped have reduced T_c due to lower doping, and not due to increased disorder. In Fig. 1 we compare the spectra for the near-optimal (87 K) and underdoped samples with an irradiated sample, whose T_c has been brought down to 79 K by intentionally disordering an 87 K material by high-energy electron irradiation. We see that the 83 K underdoped sample has a much broader normal-state spectrum that the irradiated sample with a similar T_c (Fig. 1*a*), and the 10 K sample has an even broader spectrum. Given the considerable evidence linking ARPES linewidths with electron–electron interactions[15,16], this suggests that underdoped systems are more strongly correlated.

In fact, the spectra of the underdoped sample are so broad that it is difficult to define a spectral peak above T_c. It is therefore significant to note in Fig. 1*b* that for $T \ll T_c$ the line shape sharpens up and a well defined peak is seen for the 83 K sample (at those **k**-points at which there is a sizeable superconducting gap). From Fig. 1*b* it is clear that all samples in the superconducting state have very similar low-temperature lineshapes, even though their lineshapes differ significantly in the normal state. We note that the 10 K sample is still in the normal state at $T = 14$ K, and therefore the linewidth sharpening[15] is associated with superconductivity, rather than with the temperature. Because underdoped samples have broad line shapes which are difficult to fit by any simple spectral function[11], we use the shift of the midpoint of the leading edge of a spectrum from the zero of the binding energy (that is, the Fermi energy) as an estimate of the gap. We expect, based on our earlier studies[14], that this estimate is qualitatively correct for both the magnitude and the **k**-dependence of the gap.

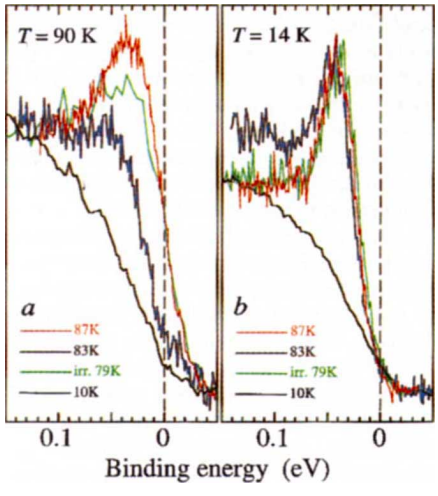

FIG. 1 ARPES spectra at the $(\pi,0)$–(π,π) Fermi surface crossing point for four samples (labelled by T_c): near-optimal (87 K, red trace), underdoped (83 K and 10 K, blue trace and black trace, respectively), and irradiated (79 K, green trace), at $T = 90$ K (*a*), and $T = 14$ K (*b*). Note that all superconducting-state spectra are similar, while the normal-state spectra differ significantly. A comparison of linewidths between the underdoped 83 K and irradiated 79 K samples suggests that disorder is not the main cause of linewidth broadening.

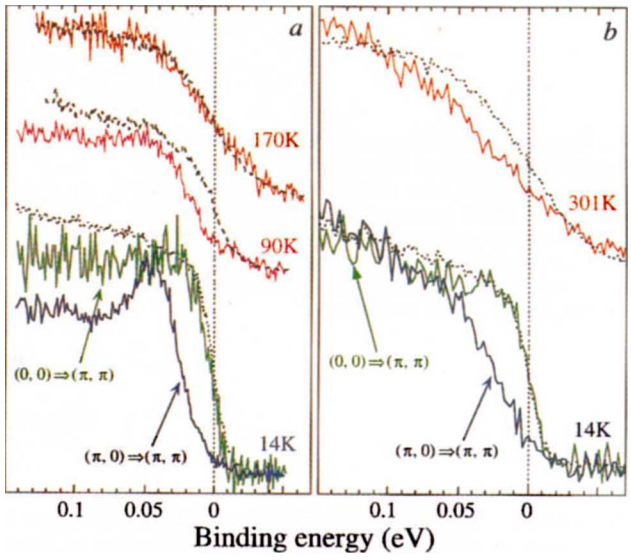

FIG. 2 Spectra (solid lines) for underdoped samples at the $(\pi,0)$–(π,π) Fermi surface crossing, along with reference Pt spectra (broken lines) at different temperatures. *a*, Spectra (22-eV photons) of the 83 K sample. At 14 K there is a gap in the superconducting state, which persists into the normal state in the 90 K spectrum, eventually closing at $T^* = 170$ K. *b*, Spectra (19-eV photons) of the 10 K sample. Note a pseudogap at the $(\pi,0)$–(π,π) Fermi surface crossing exists in the normal state from 14 to 301 K. For both *a* and *b* we also plot the spectrum at the $(\pi,0)$–(π,π) Fermi surface crossing at 14 K, showing a vanishing gap.

Spectra for the 83 K sample at three different temperatures are shown in Fig. 2*a* together with spectra (broken lines) from a polycrystalline Pt foil in electrical contact with the sample. The Pt leading-edge midpoint determines the Fermi energy. At the $\bar{M} = (\pi, 0)$ to $Y = (\pi, \pi)$ Fermi surface crossing, we find that the leading edge of Bi2212 is pushed to positive binding energies relative to Pt at 14 K indicating a large superconducting gap. This gap does not fully close above T_c, as seen in the 90 K data, and we will call this a 'pseudogap'. We use this term because the linewidths above T_c are so broad that there is non-zero spectral weight at the Fermi energy, so that a true gap does not exist. Similar results have also been recently reported in refs 17 and 18. The pseudogap persists up to 170 K, which we identify as T^*, where no visible shift is seen between the Bi2212 and Pt leading edges and the pseudogap vanishes. We contrast this behaviour to that along the (π, π) direction, where no gap is seen even well below T_c.

Above $T^* = 170$ K, the Fermi surface of the 83 K sample is recovered, by which we mean that we can experimentally map out a closed contour of gapless excitations in **k**-space. Below T^* if one makes a sequence of cuts in **k**-space normal to the Fermi surface, then those points where the gap is smallest along a cut define the minimum gap locus. For the 83 K sample, this locus is found to coincide with the Fermi surface measured above T^*, and is a large hole-like barrel enclosing the (π, π) point. Preliminary results indicate a slight reduction in the enclosed area relative to optimal doping; details will be presented in a future publication.

In Fig. 2*b* we show similar results for the 10 K sample. Again, a large pseudogap in the normal state is seen along $\bar{M}Y$ and no gap along ΓY ($r = (0, 0)$). For this sample, though, the large pseudogap does not close even at 301 K, the highest temperature at which we did measurements. Thus $T^* > 301$ K at this doping level. As a gapless Fermi surface is not recovered even at 301 K, we use the minimum gap locus (defined above) to infer the shape and size of the Fermi surface which would presumably be recovered above T^*. The minimum gap locus for the 10 K sample is a large barrel, as in the optimal and lightly-underdoped cases. Preliminary results indicate that its volume is smaller for the 10 K sample

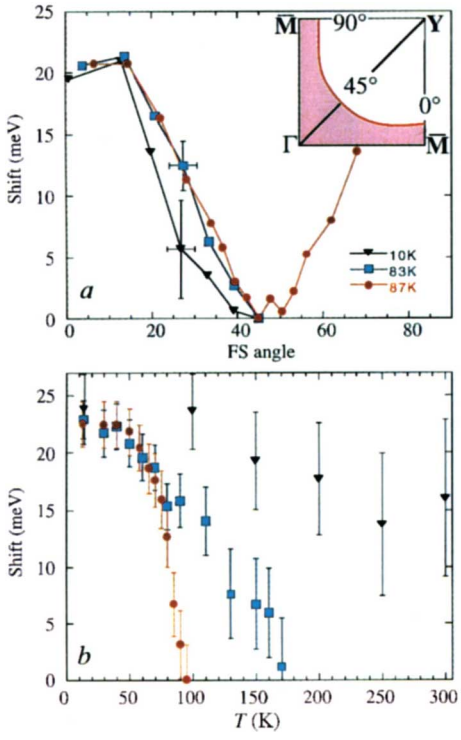

FIG. 3 Momentum- and temperature-dependence of the gap estimated from leading-edge shift (see text). *a*, **k**-dependence of the gap in the 87 K T_c, 83 K T_c and 10 K T_c samples, measured at 14 K. The inset shows the Brillouin zone with a large Fermi surface (FS) closing the (π,π) point, with the occupied region shaded. Note the striking similarity in both the magnitude and the **k**-dependence of the gap in the three samples with widely differing T_cs. *b*, Temperature dependence of the maximum gap in a near-optimal 87 K sample (circles), underdoped 83 K (squares) and 10 K (triangles) samples. Note smooth evolution of the 'gap' from superconducting to normal state for the 83 K sample.

than the 83 K sample, as expected. Note that the existence of a large Fermi surface closed about (π,π) would contradict several theories of lightly doped Mott insulators which predict small hole pockets centred above $(\pi/2,\pi/2)$.

In Fig. 3*a* we plot the angular variation of the leading-edge shifts measured from the Fermi energy at $T = 14$ K along the Fermi surface (FS). For the sake of comparison between samples, we vertically offset the shifts in Fig. 3*a* so that the shift at 45° is zero. (The offset is −3 meV for the 83 K sample and +2 meV for the 10 K sample.) We have seen similar sample-to-sample variations of the offsets for optimal-doped samples with the same T_c, so we do not regard these offsets as significant. Note the large error bars on the results for 10 K sample, as this has a rather broad spectrum at 14 K which makes it difficult to accurately determine the midpoint of its leading edge. To address the pseudogap anisotropy for the 10 K sample, we have measured its angular dependence on the locus of minimum gap just as we did for the 83 K sample.

Remarkably, both the magnitude and the **k**-dependence of the gap are similar for the three samples, and independent of carrier concentration, as seen from Fig. 3*a*, even though T_c and T^* change appreciably. The doping-independence of the pseudogap magnitude has also been suggested in ref. 19. We note that the observed shift in the 87 K sample corresponds to a superconducting gap with a maximum value of 33 meV as determined by a spectral function analysis of the data[11,14]. The **k**-dependence of the gap in all the samples is very similar to that of the near-optimal 87 K material, which has been studied in detail by our group[13,14] and found to be consistent with a *d*-wave $|\cos k_x - \cos k_y|$ gap, as suggested in earlier ARPES studies[12].

We emphasize that, as far as ARPES is concerned, there is no difference between the gap seen above and below T_c, except in one respect which we discuss below. This is clearly seen for the 83 K sample in Fig. 3*b*, where we plot the temperature dependence of the leading-edge shifts, without any offsets, at the $M = (\pi, 0)$ to $Y = (\pi, \pi)$ Fermi surface crossing for various samples. (Fig. 3*a* and Fig. 3*b* were obtained from different data sets, and therefore show slightly different values of the maximum gap). For the 83 K sample there is no signature of the phase transition at T_c in the magnitude of the gap, which eventually vanishes at $T^* = 170$ K. In contrast, in the near-optimal 87 K sample T^* (at which the gap closes) is close to T_c. As for the 10 K sample, a pseudogap regime exists over the entire range of temperatures studied. The one difference between the spectra in the superconducting and the pseudogap states is in their linewidths. Above T_c the linewidth is very broad, and spectral weight is present at the Fermi energy even though the leading edge is shifted due to the pseudogap. In contrast, well below T_c, the linewidth is resolution-limited, and a clear gap is observed, with very small spectral weight at the Fermi energy due to thermally excited quasi-particles.

These observations are remarkable and, to our knowledge, such effects have not been seen before in ordinary bulk superconductors. Part of our initial motivation was the prediction[20,21] in related model systems that the pseudogap is a normal-state precursor of the superconducting gap above T_c, where there is a pairing amplitude without phase coherence[22]. At present, however, there is no quantitative theory to explain our observations of the evolution of the planar Fermi surface, T^*, T_c and the gap as functions of the carrier concentration.

We summarize our results in the form of a phase diagram for Bi2212 in Fig. 4. At present, this is schematic, as we do not know the precise carrier concentrations for our samples, except for optimal doping, which corresponds approximately to 0.17 holes per Cu (ref. 16). (For hole concentrations in polycrystalline samples, see ref. 23.) The filled symbols denote the superconducting T_c determined by our susceptibility measurements. The full

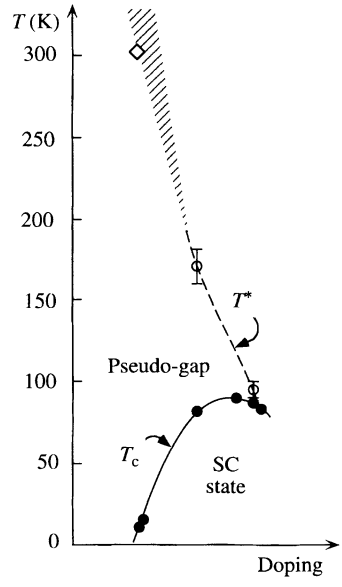

FIG. 4 Schematic phase diagram of Bi2212 as a function of doping. The filled symbols are the measured T_cs for the superconducting phase transition from magnetic susceptibiity. The open symbols are the T^* at which the pseudogap closes; for the $T_c = 10$ K sample, the symbol at 301 K is a lower bound on T^* (thus the hatching). The region between T^* and T_c is an unusual 'normal' state with a pseudogap in the electronic excitation spectrum.

line (which is a guide to the eye) through these points represents a phase boundary between the superconducting (SC) and 'normal' phases. The latter exhibits a pseudogap in its electronic excitation spectrum, which closes only at T^*. The experimental points for T^* are denoted by open symbols, and the dashed line through these points denotes a crossover line above which a Fermi surface of gapless excitations is recovered. We find that T^* increases with underdoping, consistent with earlier results[9,10], and 301 K represents only a lower bound on the T^* for our $T_c = 10$ K sample, in which T_c is lower by a factor of at least 30 relative to T^*. Given their same **k**-dependence above and below T_c, and smooth evolution through T_c, our results suggest that the normal-state pseudogap is closely related to the superconducting gap below T_c. □

Received 15 April; accepted 11 June 1996.

1. Schrieffer, J. R. *Theory of Superconductivity* (Cummings, Reading, 1964).
2. Warren, W. W. Jr *et al. Phys. Rev. Lett.* **62,** 1193–1196 (1989).
3. Takigawa, M. *et al. Phys. Rev.* B**43,** 247–257 (1991).
4. Alloul, H., Mahajan, A., Casalta, H. & Klein, O. *Phys. Rev. Lett.* **70,** 1171–1174 (1993).
5. Rossat-Mignod, J. *et al. Physica* B**186–188,** 1–8 (1993).
6. Homes, C. C., Timusk, T., Liang, R., Bonn, D. A. & Hardy, W. N. *Phys. Rev. Lett.* **71,** 1645–1648 (1993).
7. Basov, D. N., Mook, H. A., Dabrowski, B. & Timusk, T. *Phys. Rev.* B**52,** 13141–13144 (1995).
8. Loram, J. W., Mirza, K. A., Cooper, J. R. & Liang, W. Y. *Phys. Rev. Lett.* **71,** 1740–1743 (1993).
9. Tallon, J. L., Cooper, J. R., de Silva, P., Williams, G. V. M. & Loram, J. W. *Phys. Rev. Lett.* **75,** 4114–4117 (1995).
10. Batlogg, B. *et al. Physica* C**235–240,** 130–133 (1994).
11. Ding, H. *et al. Phys. Rev. Lett.* **74,** 2784–2787 (1995); **75,** 1425 (1995).
12. Shen, Z.-X. *et al. Phys. Rev. Lett.* **70,** 1553–1556 (1993).
13. Norman, M. R., Randeria, M., Ding, H., Campuzano, J. C. & Bellman, A. F. *Phys. Rev.* B**52,** 15107–15110 (1995).
14. Ding, H. *et al.* http://xxx.lanl.gov/archive/cond-mat/9603044.
15. Randeria, M. *et al. Phys. Rev. Lett.* **74,** 4951–4954 (1995).
16. Ding, H. *et al. Phys. Rev. Lett.* **76,** 1533–1536 (1996).
17. Loeser, A. G., Shen, Z.-X. & Dessau, D. S. *Physica* C**263,** 208–213 (1996).
18. Loeser, A. G. *Science* (in the press).
19. Loram, J. W., Mirza, K. A., Wade, J. M., Cooper, J. R. & Liang, W. Y. *Physica* C**235–240,** 134–137 (1994).
20. Randeria, M., Trivedi, N., Moreo, A. & Scalettar, R. T. *Phys. Rev. Lett.* **69,** 2001–2004 (1992).
21. Trivedi, N. & Randeria, M. *Phys. Rev. Lett.* **75,** 312–315 (1995).
22. Emery, V. & Kivelson, S. A. *Nature* **374,** 434–437 (1995).
23. Groen, W. A., de Leeuw, D. M. & Feiner, L. F. *Physica* C**165,** 55–61 (1990).
24. Imai, J. *et al. Physica C* **162–164,** 169–170 (1989).

ACKNOWLEDGEMENTS. This work was supported by the US NSF, the US Dept of Energy, Basic Energy Sciences, the US NSF Science and Technology Center for Superconductivity, the Japan Society for the Promotion of Science, NEDO, and the Ministry of Education, Science and Culture of Japan. The Synchrotron Radiation Center is supported by the NSF.

CORRESPONDENCE should be addressed to J.C.C. (e-mail: jcc@uicws.phy.uic.edu).

Electrical conductivity of individual carbon nanotubes

T. W. Ebbesen*, H. J. Lezec†, H. Hiura‡, J. W. Bennett*, H. F. Ghaemi* & T. Thio*

* NEC Research Institute, 4 Independence Way, Princeton, New Jersey 08540, USA
† Micrion Europe GmbH, Garmischer Strasse 4/V, 80339 München, Germany
‡ Fundamental Research Laboratories, NEC, 34 Miyukigaoka, Tsukuba 305, Japan

THE interest in carbon nanotubes has been greatly stimulated by theoretical predictions that their electronic properties are strongly modulated by small structural variations[1–8]. In particular, the diameter and the helicity of carbon atoms in the nanotube shell are believed to determine whether the nanotube is metallic or a semiconductor. Because of the enormous technical challenge of making measurements on individual nanotubes, however, experimental studies have been limited mainly to bulk measurements[9], which indicate only that a fraction of the nanotubes are metallic or narrow-band semiconductors[10]. Recently, measurements of the magneto-conductance of a single multi-shell nanotube in a two-probe configuration showed that the transport is characterized by disorder and localization phenomena[11]. To avoid possible ambiguities due to poor sample contacts, four-probe measurements are needed. Here we report four-probe measurements on single nanotubes made by lithographic deposition of tungsten leads across the tubes. We find that each multi-shell nanotube has unique conductivity properties. Both metallic and non-metallic behaviour are observed, as well as abrupt jumps in conductivity as the temperature is varied. The differences between the electrical properties of different nanotubes are far greater than expected. Our results suggest that differences in geometry play a profound part in determining the electronic behaviour.

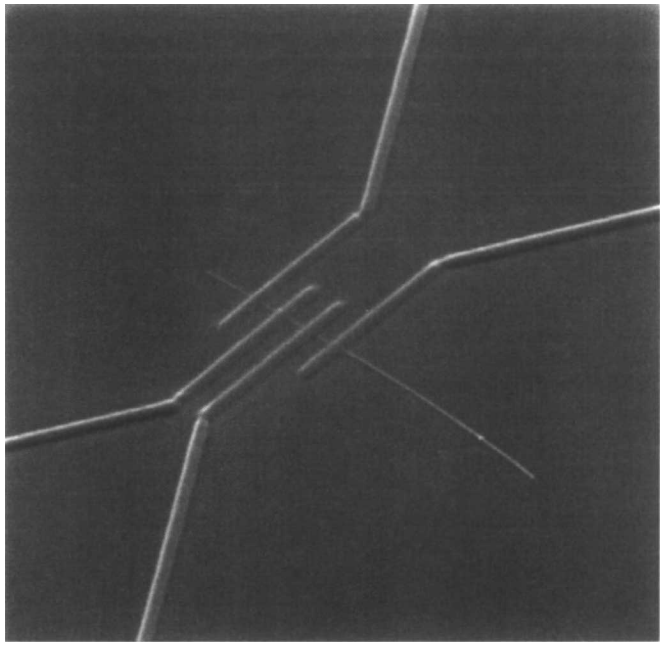

FIG. 1 A single nanotube connected to four 80-nm wide tungsten wires and imaged by FIB.

The carbon nanotubes were prepared by the carbon-arc method[12] which yields nanotubes with the highest degree of structural integrity and then further annealed at 3,120 K for 15 min under argon. This high-temperature treatment eliminates many defects as seen by electron spin resonance spectroscopy[10]. The nanotubes were spread on an oxidized silicon surface between gold pads. Using a Micrion focused-ion-beam (FIB) System 9100 (30 keV Ga ions, 10 nm nominal spot diameter), the surface was visualized using a low beam current (4 pA) in search of a nanotube with the right length (~2–4 μm). The total dose during this imaging was 2×10^{14} ions per cm^2 (that is, two ions per 100 $Å^2$). Once found, four 80-nm-wide tungsten leads were patterned on the nanotube by ion-induced deposition of tungsten from a $W(CO)_6$ carrier gas. The patterning is performed under computer control without further visualizing the sample. All the samples were prepared with exactly the same procedure and doses. An example of the resulting connections is shown in Fig. 1. These small leads were then connected to four surrounding gold pads. The distance between the contacts on the nanotube is in all cases between 0.3 and 1.0 μm. It was verified that with such spacings the resistance between the leads (without the nanotube) was larger than the limit of our measurement, 10 GΩ. The diameter of each nanotube was measured with a Nanoscope III atomic force microscope. The four-probe resistances were measured in d.c. using a Keithley 220 current supply and either a Keithley 196 multimeter or a Keithley 617 electrometer, depending on the sample resistances. The applied voltage was held below 1 V at all